High-throughput and clogging-free microfluidic filtration platform for on-chip cell separation from undiluted whole blood

Yinuo Cheng, Xiongying Ye,[a] Zengshuai Ma, Shuai Xie, and Wenhui Wang
State Key Laboratory of Precision Measurement Technology and Instruments, Department of Precision Instruments, Tsinghua University, Beijing, China

(Received 24 December 2015; accepted 3 February 2016; published online 12 February 2016)

Rapid separation of white blood cells from whole blood sample is often required for their subsequent analyses of functions and phenotypes, and many advances have been made in this field. However, most current microfiltration-based cell separation microfluidic chips still suffer from low-throughput and membrane clogging. This paper reports on a high-throughput and clogging-free microfluidic filtration platform, which features with an integrated bidirectional micropump and commercially available polycarbonate microporous membranes. The integrated bidirectional micropump enables the fluid to flush micropores back and forth, effectively avoiding membrane clogging. The microporous membrane allows red blood cells passing through high-density pores in a cross-flow mixed with dead-end filtration mode. All the separation processes, including blood and buffer loading, separation, and sample collection, are automatically controlled for easy operation and high throughput. Both microbead mixture and undiluted whole blood sample are separated by the platform effectively. In particular, for white blood cell separation, the chip recovered 72.1% white blood cells with an over 232-fold enrichment ratio at a throughput as high as 37.5 μl/min. This high-throughput, clogging-free, and highly integrated platform holds great promise for point-of-care blood pretreatment, analysis, and diagnosis applications. © *2016 AIP Publishing LLC*.
[http://dx.doi.org/10.1063/1.4941985]

I. INTRODUCTION

White blood cells (WBCs) contain rich information about the functionality of the human immune system.[1] Many analyses on WBCs require their prior separation from whole blood, to remove the possible interference from the presence of red blood cells (RBCs) and platelets.[2] In human blood, RBCs outnumber WBCs approximately at a ratio of 1000:1, and the blood cell concentration is extremely high.[1] Owing to the high blood cell concentration and relatively low abundance of WBCs in blood, efficient on-chip separation of WBCs from undiluted whole blood is of great challenge. Many strategies have been developed for cell separation and as described in the literature,[3–5] they could be categorized into active and passive approaches. In short, the former strategies rely on an external force field for functionality, while the latter rely entirely on the channel geometry and/or inherent hydrodynamic forces for functionality.[3,6] Active strategies include fluorescence-activated cell sorting,[7] magnetic sorting,[8] dielectrophoresis,[9] and so on. Passive strategies include obstacle induced separation,[10–12] hydrodynamic separation,[13–15] pinched flow fractionation,[16,17] inertial microfluidic separation,[18–20] and microfiltration.[21–23] Microfiltration is among the few separation approaches that do not require pretreatment steps or external force field for functionality. Furthermore, it is a label-free method and easily integrated with downstream analysis device, so cell separation based on

[a]Author to whom correspondence should be addressed. Electronic mail: xyye@mail.tsinghua.edu.cn

microfiltration is adopted in this paper. The microfiltration devices for cell separation include weir-type,[24,25] pillar-type,[26,27] and membrane-type,[22,28–30] and they can be further classified into dead-end filtration[22] and cross-flow filtration[2,21,23] based on the direction of the main flow to the filter. Continuing efforts in microfluidic commercialization have also resulted in cost effective, commercially available microporous membranes which could readily be embedded in microfluidic chips for easy-to-build, large filtration foot-print, and high-throughput cell separation chip.

Hosokawa *et al*. presented a microfluidic device equipped with a microfiltration membrane for the separation of WBCs. The dead-end device could recover over 90% WBCs from diluted blood sample, but with low processing capability of less than 1 μl blood sample. One big problem came from the microporous membrane clogging with blood cells.[31] Wei *et al*. presented a microfluidic particle sorting chip with an integrated PDMS membrane that is porous at defined areas. This allows for simultaneous valving and filtering functionality. Membranes with pores as small as 6.4 μm were fabricated on a mold, and smaller pores were formed by overlapping two or more such porous membranes with planar offset. The device separated WBCs and human leukemia cells from whole blood at a throughput of around 3 μl/min.[32] Later, this sorting chip was extended to the separation of hematopoietic stem cells from diluted bone marrow samples by the same group. Because stem cells are so rare, the new chip has a larger parallelogram-shaped separation area to handle relatively large amounts of fluid, and the throughput was scaled up to 17.2 μl/min.[33] Featuring with surface micromachined membranes, Li *et al*. demonstrated a microfluidic device for continuous-flow isolation and sorting of WBCs from whole blood. Taking advantage of the cross-flow filtration scheme and high porosity of the microfiltration membranes, the device could recover 27.4% WBCs at a sample throughput of 16.7 μl/min.[34] The membrane-type based devices for cell separation face the limitations of membrane clogging and relatively low throughput. Besides, the overwhelming majority of the reported microfiltration devices required external fluid-driving sources, such as syringe pumps,[22,34,35] peristaltic pumps,[30,31,36] and vacuum pumps,[10,37] and they will obstruct the entire system's miniaturization.

To overcome the main problems of micropores clogging, relatively low throughput, and external fluid-driving source requirement, a microfiltration chip with an integrated rotary bidirectional micropump and an embedded polycarbonate (PC) microporous membrane for cell separation is demonstrated herein. The chip works with cross-flow filtration mode combining with dead-end filtration mode. The micropump not only serves as a fluid-driving source but also provides the ability to rapidly change the flow direction in order to flush micropores in reverse direction and effectively avoid clogging of the membrane. Separation of two-size polystyrene (PS) microbeads and WBCs from whole blood is demonstrated and the separation performance is evaluated for optimization by studying key parameters of the chip. All the separation processes, including blood and buffer loading, separation, and sample output, are automatically realized. This microfiltration chip with high throughput could be easily integrated with downstream components for on-chip analysis.

II. THE MICROFILTRATION CHIP

A. Design

As shown in Fig. 1, the microfiltration chip is composed of a rotary pump, four valves, filtration region, channels, an inlet, and two outlets (Fig. 1(a)). Basically, the filtration region has two fluidic chambers separated by a microporous membrane which acts as a sieve to filter RBCs and platelets out of the whole blood sample pumped into the bottom chamber (Fig. 1(b)). After one run, filtered RBCs and platelets flow through the top chamber and outflow from the waste outlet. The chip has five structured layers (Fig. 1(c)), starting from the bottom including a bottom fluidic channel layer (BFL), an adhesive layer (AL), a PC microporous membrane layer (ML), a top fluidic channel layer (TFL), and a top PDMS membrane layer (TL). BFL is the base of the chip, providing channels for the blood sample to flow in a loop during filtration. Above the snake-shaped channel area of BFL is a recess that allows ML fitting with BFL through AL. TFL is then used to fully cover the filtration membrane and has a same-snake-

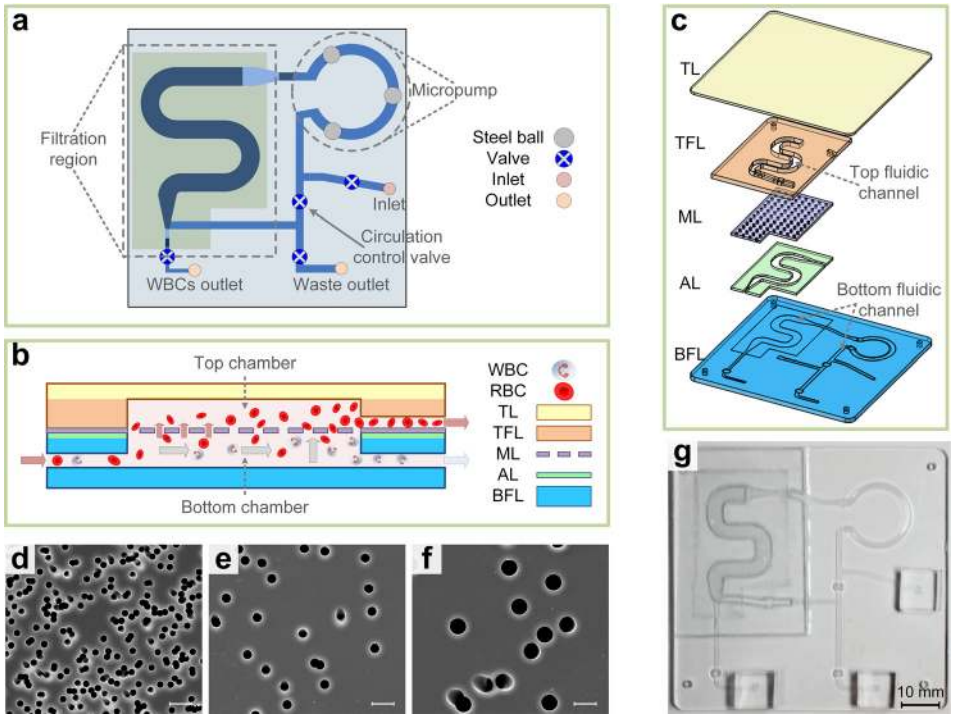

FIG. 1. The microfiltration chip. (a) Schematic of the chip, (b) cross-section of the chip in the filtration region, (c) explosive view of multilayer structure of the chip, starting from the bottom: bottom fluidic channel layer (BFL), adhesive layer (AL), PC microporous membrane layer (ML), top fluidic channel layer (TFL), and top PDMS membrane layer (TL), (d)–(f) scanning electron microscope (SEM) images of a polycarbonate microporous membrane with pore sizes of 3 μm, 5 μm, and 8 μm, respectively, (g) photograph of the fabricated microfiltration chip. Scale bars in (d)–(f) represent 10 μm.

shaped channel to form the top chamber which flows away the filtered RBCs and platelets to the waste outlet. Note here that TFL is larger than ML especially in the snake-tail area such that a connection is established between the top fluidic channel and channel on the BFL. Finally, a PDMS membrane (TL) is used to fully cover TFL and BFL to form closed fluidic channels. Ideally, liquid exchange between the bottom fluidic channel and the top fluidic channel occurs only in the filtration region. However, in practice, extra care is taken to make the right edge of TFL tightly bonded with TL to avoid any cross-talk that would otherwise occur between the snake-shape head and tail channels on the BFL due to poor bonding. The fluidic channels on the BFL are designed to be 1.4 mm wide and 0.12 mm deep, and the filtration region channels on the BFL are designed to be 2.6 mm wide, 0.1 mm deep, and 50 mm long. The ~20 μm thick PC microporous membrane is sandwiched between the 50 μm thick AL and 142 μm thick TFL. With the current design, the effective filtration area reaches 200 mm^2, and the channel volume capacity of the microfiltration chip is totally 130 μl. Figs. 1(d)–1(f) show scanning electron microscope (SEM) images of a polycarbonate microporous membrane with pore sizes of 3 μm, 5 μm, and 8 μm, respectively.

Inspired by the pumping method developed by Quake group,[38] the micropump is another key component and composed of an annular channel covered by a flexible PDMS membrane which is pressed by three steel balls driven by a direct-current motor.[39,40] The flexible PDMS membrane peristaltically deforms by the circular movement of the balls, and the peristaltic deformation of the membrane drives the fluid flow in the channel. The flow rate of the micropump can be adjusted by changing the rotation speed of the motor. By controlling the motor to rotate reversely, the fluid flows backward, which flushes the cells trapped in micropores and avoids clogging of the membrane.[41] The chip works with cross-flow filtration mode at the front filtration region combining with dead-end filtration mode at the posterior filtration region.

B. Fabrication

The BFL made of polymethyl methacrylate (PMMA) is fabricated by a computer numerically controlled (CNC)-machine, while the AL and the TFL made of double-sided adhesive tapes (ARclear 8932 and ARseal 90880, respectively, Adhesives Research) and the ML made of PC microporous membrane are patterned by a laser cutting machine. The AL, ML, and TFL are precisely assembled onto the BFL in sequence. The TL is a 120 μm thick PDMS membrane, which is prepared by spin-coating PDMS precursor (Sylgard 184, Dow Corning, base and the crosslink reagent at 10:1 mass ratio) on a polyimide film and then baking 3 h at 80 °C. The PDMS membrane is bonded to the assembled PMMA layer by chemical surface modification of the PMMA layer via 3-amino-propyltriethoxysilane (APTES), followed by plasma activation of the PDMS membrane and the modified PMMA layer as previously described in the literature.[21,42] Then, the polyimide film is peeled off. Because the layers of TFL, ML, and AL sandwiched by bigger TL and BFL, there exist opening gaps along the edge of TFL after initial bonding. To prevent any liquid leakage, PDMS prepolymer is injected to seal the gaps. Finally, 2 mm thick PDMS blocks are bonded on top of the TL by plasma activation, and holes through the blocks are punched using a 1.3 mm diameter punch to form the inlet and outlets. Fig. 1(g) shows a picture of the fabricated microfiltration chip.

C. Working procedure

The cell separation starts with sample loading, in which a volume of buffer is loaded via the inlet to rinse the chip (Fig. 2(a)), followed by a volume of whole blood sample (Fig. 2(b)) and then another volume of buffer (Fig. 2(c)). Note here the volume of whole blood sample is controlled precisely such that the membrane pores could not be fully blocked. And the external motor is controlled to rotate in one direction (e.g., anti-clockwise) to make fluid flow forward. During sample loading, the whole blood is transported to the filtration region, where WBCs are stopped by the microporous membrane and gather in the tail of snake-shaped channel, while RBCs and platelets pass through the membrane and flow out from the waste outlet.

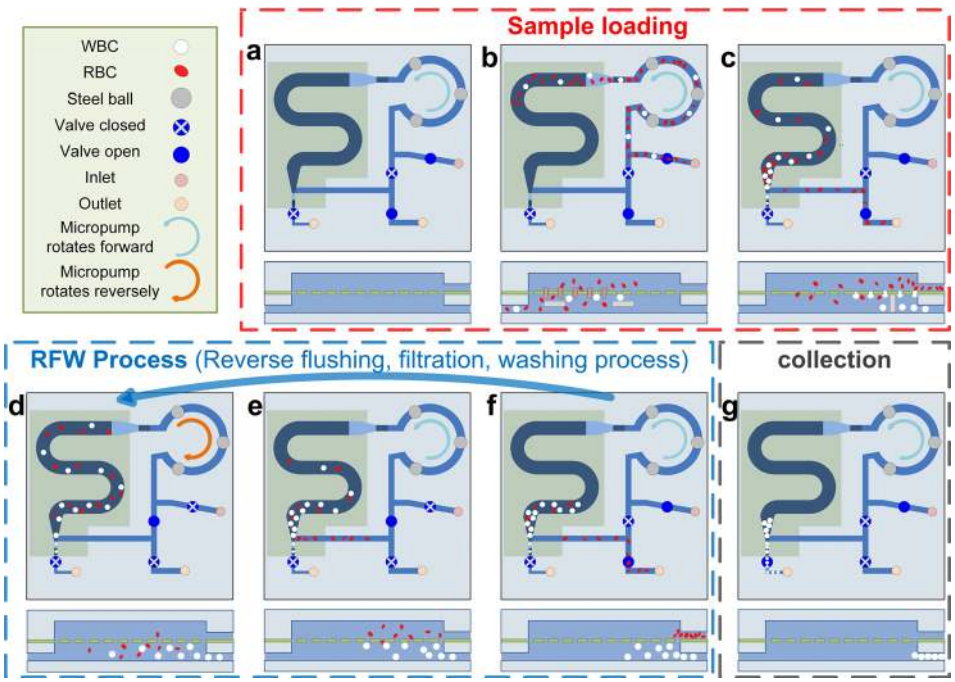

FIG. 2. Working procedure for cell separation. (a) Load buffer, (b) load whole blood, (c) load buffer, (d) reverse flushing, (e) circulating filtration, (f) washing away remaining RBCs and platelets, (g) collect WBCs sample.

After sample loading, the chip works repeatedly in a reverse flushing, filtration, and washing process (RFW process) till the filtration is satisfactory. During this process, first all the inlet and outlet valves are closed, and the circulation control valve is opened. In the meantime, the external motor is controlled to rotate reversely (e.g., clockwise) such that the fluid flows backward. In this way, the cells trapped in micropores are flushed away and back to the bottom chamber (Fig. 2(d)), thus avoiding blocking of the membrane. With clear micropores, the micropump rotates forward again to resume separation by internal fluidic circulation without extra buffer (Fig. 2(e)). After the sample goes through the filtration region, a washing step is performed by pumping in buffer to purge the filtered RBCs and platelets via the waste outlet (Fig. 2(f)). This RFW process is repeated several times to further improve the separation performance.

Once the separation is satisfactory to our demand, the WBCs are collected via the WBCs outlet (Fig. 2(g)).

III. EXPERIMENTAL METHODS

A. Materials

Isopore PC membranes with pore sizes of 8 μm (TETP04700, 18 μm thick, 5%–20% porosity), 5 μm (TMTP04700, 20 μm thick, 5%–20% porosity), and 3 μm (TSTP04700, 22 μm thick, 11% porosity) are purchased from Millipore (Canada). APTES used for silanization is purchased from J&K Scientific Ltd. (China). Suspensions of PS microbeads (10 μm, 2×10^4 beads/μl and 3 μm, 7×10^5 beads/μl) are purchased from Knowledge & Benefit Sphere Tech. Co., Ltd. (China). The 10 μm and 3 μm microbead mixture is prepared in deionized (DI) water with a 1:185 number ratio for 10 μm and 3 μm microbeads at a concentration of 4×10^4 beads/μl. Collected from healthy donors and stored in a collection tube containing EDTAK2, whole blood sample is maintained at 4 °C and is used within 8 h in separation experiments. The buffer used for cell separation is phosphate-buffered saline (PBS) (E607008, Sangon Biotech, China), while for microbeads separation is DI water. FITC (Fluorescein isothiocyanate)-labeled anti-CD45 antibody is obtained from Mindray Medical International Ltd. (China).

B. Setup

The experimental setup for separation is depicted in Fig. 3. It mainly includes the rotary bidirectional motor for microfluidic pumping, four electromagnets for valve control, and microfiltration chip for fluidic sample processing. On the motor head are evenly mounted three steel balls, which are set in contact with the PDMS membrane-covered annular channel to pump fluid. To control the valves, four electromagnets are set above the PDMS membrane at designed points of the channels. Working as a mechanical contact switch, the electromagnet deforms the PDMS membrane to close the valve when power is "on." A portable home-made control system

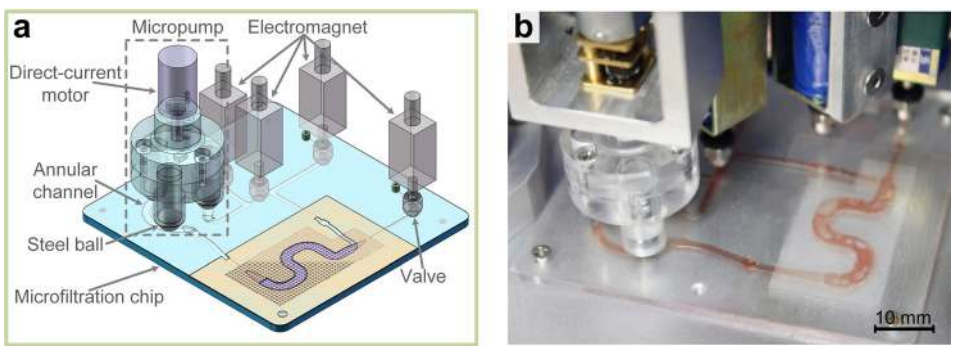

FIG. 3. Microfluidic cell separation platform. (a) A schematic including the micropump, electromagnets, and microfiltration chip and (b) a photograph of the setup operating with a whole blood sample.

controls the motor and electromagnets to accomplish the separation procedure, and the motor rotation speed and direction are accurately controlled.

A fluorescence microscope with a digital camera (Leica DM2500 M & Leica DFC450C Digital Camera, Germany) is used for experiment observation and image recording. After whole blood separation, the collected samples are stained with 10 μl FITC-labeled anti-CD45 antibody at 20 °C for 15 min. The numbers of cells and microbeads within the collected samples are obtained by microscopic analysis using ImageJ software (National Institutes of Health, USA) and manual counting, and averaged over three to five different microscopic images. A hematology analyzer (BC-5800, Mindray Medical International Ltd., China) is used to measure the WBCs and RBCs concentrations.

C. Performance evaluation

In line with the literature, four separation performance metrics, i.e., enrichment ratio, purity, recovery rate, and removal efficiency, are utilized to evaluate the separation performance in this paper. Defining metrics will help us to explore the practical trade-offs, for instance, enrichment ratio versus recovery rate. Enrichment ratio is a fairly standardized metrics to describe the enrichment of target cells from a sample, while purity is used to describe separation result and may vary significantly based on definition. Recovery rate is often used to describe losses of target cells either to leakage or retention within the chip, and removal efficiency is reported to describe the removal of undesired cells. They are defined by[4,24]

$$Enrichment\ ratio = (N_{\text{tar-out}}/N_{\text{und-out}})/(N_{\text{tar-in}}/N_{\text{und-in}}), \tag{1}$$

$$Purity = N_{\text{tar-out}}/(N_{\text{tar-out}} + N_{\text{und-out}}) \times 100\%, \tag{2}$$

$$Recovery\ rate = N_{\text{tar-out}}/N_{\text{tar-in}} \times 100\%, \tag{3}$$

$$Removal\ efficiency = (N_{\text{und-in}} - N_{\text{und-out}})/N_{\text{und-in}} \times 100\%, \tag{4}$$

where $N_{\text{tar-out}}$ is the number of target cells in the collection outlet, $N_{\text{und-out}}$ is the number of undesired cells in the collection outlet, $N_{\text{tar-in}}$ is the number of target cells in the inlet, and $N_{\text{und-in}}$ is the number of undesired cells in the inlet.[4] For these four separation performance metrics, the more useful metrics varies depending on the specific application.

IV. EXPERIMENTAL RESULTS

A. Characteristics of the micropump

It is vital to know the relationship between the motor rotation speed and the flow rate. To this end, we utilize a simple but effective setup to characterize the micropump (Fig. 4(a)). Essentially, a horizontal scaled silicone tube is connected in the fluidic circuit. A CCD camera is mounted above the tube to measure the flow meniscus and hence calculate the flow rate. We

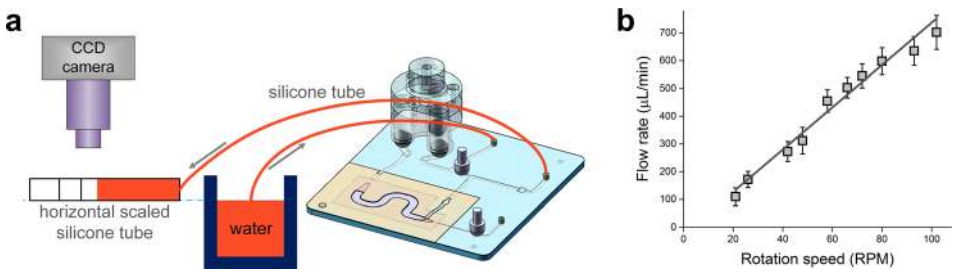

FIG. 4. Characteristics of the micropump. (a) Schematic of the setup for flow rate testing and (b) the relationship between flow rate and rotation speed of the driving motor at zero back pressure. Error bars in (b) represent standard deviations of 3 separate trials.

keep the WBCs outlet valve and the circulation control valve closed, and the water level of the inlet container and the outlet tube is maintained in the same horizontal level to guarantee zero back pressure. By changing the motor rotation speed from 21 rotation per minute (RPM) to 102 RPM, the flow rate is increased from ∼172 μl/min to ∼702 μl/min at a linear relationship (Fig. 4(b)).

B. Optimization of flow rate and micropore size

To demonstrate the effectiveness of the microfiltration chip, we conducted separation experiment with both microbead mixture and blood sample as a proof-of-concept. To evaluate the effect of flow rate on separation performance, four different flow rates of 110 μl/min, 308 μl/min, 545 μl/min, and 702 μl/min are used for both microbead mixture and whole blood sample. Microporous membranes with 8 μm pores are used as filter membranes for microbead mixture separation, while microporous membranes with 5 μm and 3 μm pores are used subsequently for whole blood separation. After filling the chip with buffer and then loading 100 μl microbead mixture, separation is implemented by continuously introducing 1.2 ml buffer with different flow rates. Fig. 5(a) shows the experimental results for microbeads separation, including enrichment ratio, recovery rate, and removal efficiency with different flow rates. The enrichment ratio increases quickly with flow rate and achieves 52-fold at 702 μl/min compared with 8-fold at 110 μl/min, while the removal efficiency increases slowly with flow rate and achieves a rather high level even at a low flow rate, indicating that this chip can effectively remove 3 μm beads. The recovery rate declines slightly with flow rate and remains over 96% for all flow rates. This under-100% recovery rate is due to irregular dispersion of the nominal 8 μm micropores and some pores join together to form pores bigger than 8 μm. An increasing flow rate generates greater hydrodynamic forces that would squeeze more beads pass through the pores. However, the high recovery rate benefits from the PS microbeads having no deformability, and there are only very few 10 μm beads passing through the micropores of the microporous membrane even under high flow rate and high pressure.

For whole blood separation, after filling the chip with PBS buffer and then loading 300 μl whole blood, separation is continued through introducing 1.2 ml PBS buffer. Figs. 5(b) and 5(c)

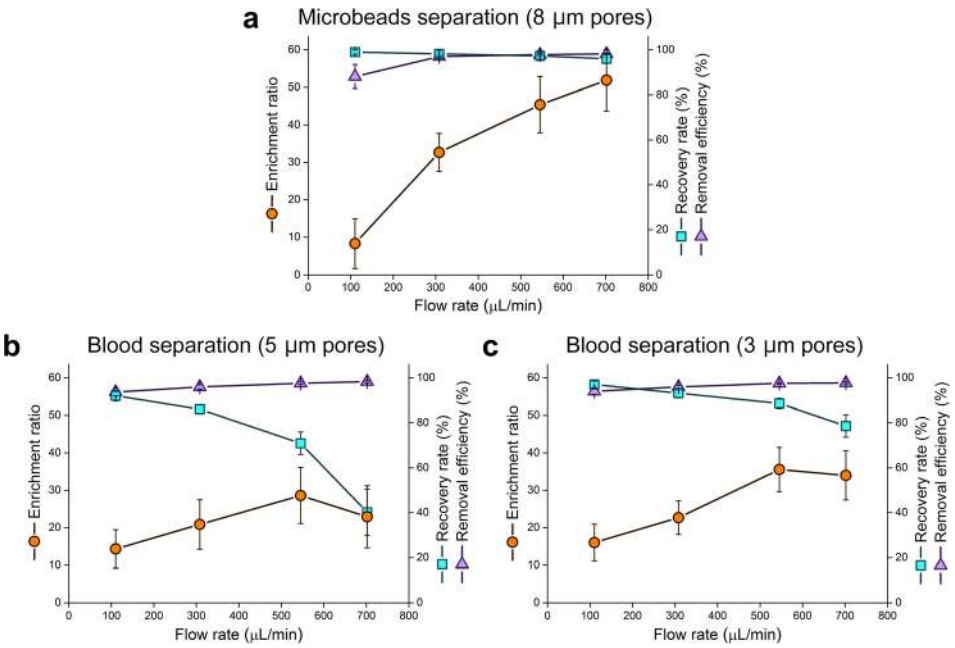

FIG. 5. Separation performance for different flow rates and pore sizes. (a) Results for microbeads separation using 8 μm pores, (b) results for whole blood separation using 5 μm pores, (c) results for whole blood separation using 3 μm pores. Error bars represent standard deviations of 5 different trials.

show the experimental results with different flow rates using microporous membranes with 5 μm pores and 3 μm pores, respectively. Different from microbead mixture separation, for cell separation, the enrichment ratio first increases with flow rate, achieves the maximum at 545 μl/min, and then turns to decrease. The recovery rate decreases with flow rate and shows a noticeable decline after 545 μl/min, indicating that there are more WBCs passing through the microporous membrane at higher flow rate. This is reasonable considering that a higher flow rate results in a higher pressure drop between the two sides of the microporous membrane, which deforms WBCs to a higher extent. Though RBCs are quickly removed at a higher flow rate, the ratio of the WBCs leaking through the microporous membrane to the removed RBCs increases. This ratio is inversely changed to the numerator of the enrichment ratio (Equation (1)); thus, its increase leads to a drop of the enrichment ratio. The removal efficiency increases continuously with flow rate as expected, and at a slower pace compared with bead separation. In order to maximize the flow rate without sacrificing the enrichment ratio and the recovery rate, a flow rate of 545 μl/min is selected in the subsequent experiments.

By comparing the three separation performance metrics in Figs. 5(b) and 5(c) under the same flow condition, both the enrichment ratio and the recovery rate in Fig. 5(c) are significantly larger than that in Fig. 5(b). Compared with microporous membrane with 5 μm pores, less WBCs leak through the membrane with 3 μm pores, so the microporous membranes with 3 μm pores are more suitable to be integrated in the microfiltration chip for the separation of WBCs from the whole blood.

C. Separation of microbeads

To optimize the separation performance, experiments with different repeating cycles of the reverse flushing, filtration, and washing process (abbreviated to RFW process) are conducted. After filling the chip with 130 μl buffer, 100 μl mixture is loaded, and initial separation is carried out by continuously introducing 1.2 ml buffer in 135 s. The RFW process, with reverse flushing for 10 s, circulating for 30 s, and washing for 20 s, is repeated several times during the separation. Fig. 6 shows the separation results with different repeating cycles of RFW process. With more cycles, the microscopic images of collected bead mixture show decreasing number of 3 μm beads, suggesting increasing enrichment of 10 μm target beads (Figs. 6(a)–6(f)). Figs. 6(g) and 6(h) show the enrichment ratio and the recovery rate of 10 μm bead, respectively. Although the recovery rate slightly decreases, the enrichment ratio increases significantly with the repeating cycles of RFW process, indicating that the RFW process is effective to improve the separation performance. For initial microbead mixture $N_{\text{tar-in}}/N_{\text{und-in}} = 1/185$, hence $\textit{enrichment ratio} = 185 \times (N_{\text{tar-out}}/N_{\text{und-out}})$, when few 3 μm microbeads remain in the separated sample, the enrichment ratio will be extremely high. After 5 cycles of RFW process, an 1858-fold enrichment ratio, a 90.7% recovery rate, and a 90.9% purity of 10 μm bead are achieved with over 99.9% 3 μm microbeads removed. The enrichment ratio and purity could be further enhanced by increasing the repeating cycles of RFW process while sacrificing the recovery rate.

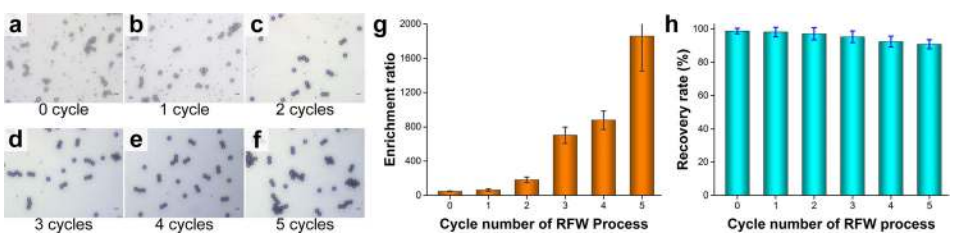

FIG. 6. Microbeads separation results with different repeating cycles of the reverse flushing, filtration, and washing process (abbreviated to RFW process). (a)–(f) Microscopic images of initial mixture and collected samples at WBCs outlet with 0–5 repeating cycles of RFW process, (g) enrichment ratio of 10 μm bead versus repeating cycles of RFW process, (h) recovery rate of 10 μm bead versus repeating cycles of RFW process. Error bars in (g) and (h) represent standard deviations of 3 different trials, and scale bars in (a)–(f) represent 10 μm.

D. Separation of WBCs from whole blood

Following the same procedure as microbeads separation, 300 μl whole blood is separated using microporous membranes with 3 μm pores, the RFW process being repeated 1–5 times, and less than 3 ml PBS buffer is used during the separation. Photographs of the separation process taken at 36 s, 130 s, and 270 s show clearly the removal of the RBCs indicated by the dimming of the sample red color (Figs. 7(a)–7(c)). The enrichment ratio of WBCs increases (Fig. 7(d)) with the repeating cycles of RFW process and the recovery rate declines slowly (Fig. 7(e)). An over 232-fold enrichment ratio of WBCs and a 72.1% recovery rate of WBCs are achieved with 99.7% RBCs removed after 5 cycles of the RFW process. Fig. 7(f) shows sample of undiluted whole blood, sample output from waste outlet, and collected WBCs sample. Fig. 7(g) is a fluorescent image of the collected sample after separation, on which the green spots indicate the stained WBCs, and Fig. 7(h) shows its corresponding bright-field image. During experiments, the separation proceeds smoothly without any substantial speed decrease, indicating that clogging is effectually prevented by reverse flushing. The purity of WBCs is 15.1%, indicating that there are still RBCs remaining in the sample. This happens because the channel right before the WBCs outlet valve acts as a "harbor" for all cells in the sample to stay away from the filtration region. It could be improved by reducing the volume of WBCs outlet channel and optimizing the separation procedure. In this experiment, separating WBCs from 300 μl undiluted whole blood only takes 8 min, equivalent to a throughput of 37.5 μl/min, which is a rather high value compared with currently reported microfluidic blood separation systems.[23,32–34]

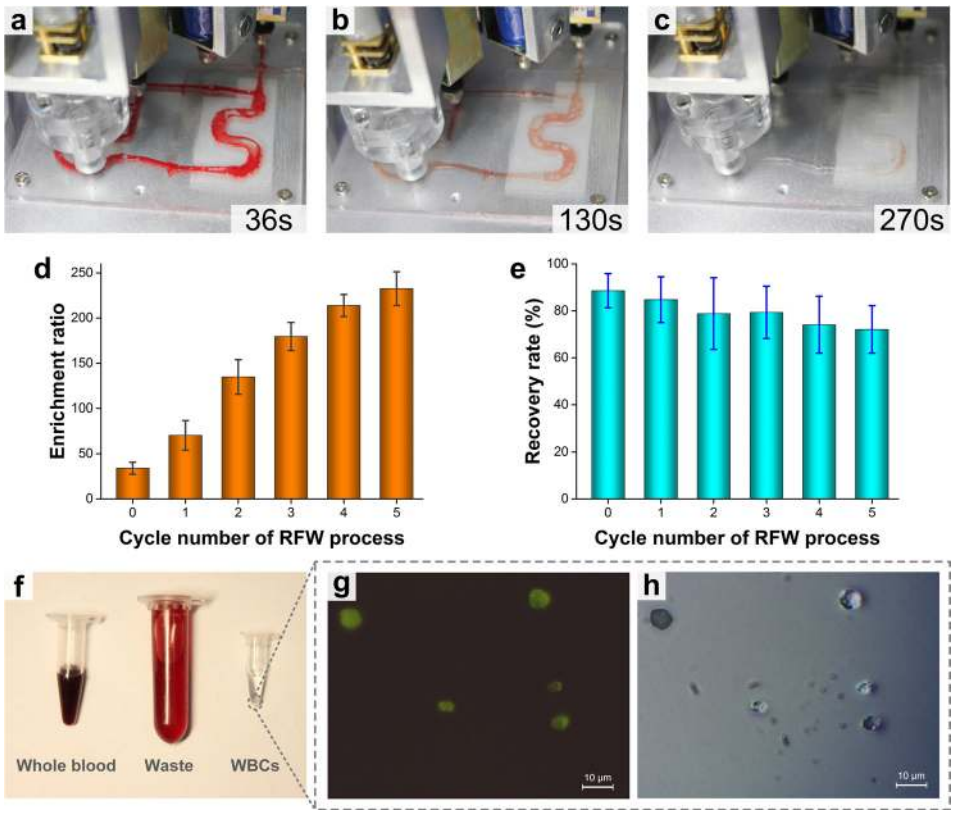

FIG. 7. Separation of WBCs from undiluted whole blood. (a)–(c) Photograph of the separation process taken at 36 s, 130 s, and 270 s, respectively, (d) and (e) enrichment ratio and recovery rate of WBCs versus repeating cycles of RFW process, respectively, (f) undiluted whole blood and its products after separation, (g) fluorescent image of WBCs collected after separation and stained with FITC-labeled anti-CD45, (h) corresponding bright-field image. Error bars in (d) and (e) represent standard deviations of 5 different trials.

V. CONCLUSIONS

In this paper, a microfluidic filtration platform with an integrated rotary bidirectional micropump was demonstrated for the separation of WBCs from undiluted whole blood with high throughput. Enabled by the bidirectional driving capability of the micropump, the cells trapped in micropores of the membrane can be easily retracted to prevent membrane clogging. All the separation processes, including blood and buffer loading, separation, and sample collection, are automatically controlled. We deliberately validated the separation performance of the chip under different flow rates, using microporous membranes with different pore size for separating microbeads mixture and whole blood. An 1858-fold enrichment ratio and 90.9% purity of 10 μm bead and a 99.9% removal efficiency of 3 μm bead were achieved for microbead separation. When separating WBCs from undiluted whole blood, the microfiltration chip with an embedded 3 μm pore size microporous membrane recovered 72.1% WBCs with an over 232-fold enrichment ratio at a throughput as high as 37.5 μl/min, meanwhile, more than 99.7% RBCs were removed. We believe the virtues of being high-throughput, clogging-free, and highly integratable make the filtration platform quite appealing, especially for rapid blood pretreatment, analysis, and diagnosis. Future work will focus on improving the enrichment ratio and purity of WBCs through further optimizing the chip structure and separation procedure.

ACKNOWLEDGMENTS

This work was supported by National Instrumentation Program (2013YQ19046701), the NSFC (Grant No. 61376120), and the One-Thousand Young Talent Program of China. The authors would like to thank for the help of blood cell measurement from Beijing Shen Mindray Medical Electronics Technology Research Institute CO., LTD.

[1]M. Toner and D. Irimia, Annu. Rev. Biomed. Eng. **7**, 77 (2005).
[2]V. Vandelinder and A. Groisman, Anal. Chem. **79**, 2023 (2007).
[3]A. A. S. Bhagat, H. Bow, H. W. Hou, S. J. Tan, C. T. Lim, and J. Han, Med. Biol. Eng. Comput. **48**, 999 (2010).
[4]D. R. Gossett, W. M. Weaver, A. J. Mach, S. C. Hur, H. Tat, K. Tse, W. Lee, H. Amini, and D. Di Carlo, Anal. Bioanal. Chem. **397**, 3249 (2010).
[5]N. Pamme, Lab Chip **7**, 1644 (2007).
[6]Z. T. F. Yu, K. M. Aw Yong, and J. Fu, Small **10**, 1687 (2014).
[7]M. M. Wang, E. Tu, D. E. Raymond, J. M. Yang, H. Zhang, N. Hagen, B. Dees, E. M. Mercer, A. H. Forster, I. Kariv, P. J. Marchand, and W. F. Butler, Nat. Biotechnol. **23**, 83 (2005).
[8]S. Miltenyi, W. Muller, W. Weichel, and A. Radbruch, Cytometry **11**, 231 (1990).
[9]I. Doh and Y. H. Cho, Sens. Actuators, A **121**, 59 (2005).
[10]R. S. Pawell, D. W. Inglis, T. J. Barber, and R. A. Taylor, Biomicrofluidics **7**, 056501 (2013).
[11]T. Krüger, D. Holmes, and P. V. Coveney, Biomicrofluidics **8**, 054114 (2014).
[12]J. A. Davis, D. W. Inglis, K. J. Morton, D. A. Lawrence, L. R. Huang, S. Y. Chou, J. C. Sturm, and R. H. Austin, Proc. Natl. Acad. Sci. U.S.A. **103**, 14779 (2006).
[13]M. Yamada and M. Seki, Lab Chip **5**, 1233 (2005).
[14]S. Sugaya, M. Yamada, and M. Seki, Biomicrofluidics **5**, 024103 (2011).
[15]S. Torino, M. Iodice, I. Rendina, G. Coppola, and E. Schonbrun, Biomicrofluidics **9**, 064107 (2015).
[16]T. Morijiri, S. Sunahiro, M. Senaha, M. Yamada, and M. Seki, Microfluid. Nanofluid. **11**, 105 (2011).
[17]J. Takagi, M. Yamada, and M. Seki, Lab Chip **5**, 778 (2005).
[18]J. Sun, C. Liu, M. Li, J. Wang, Y. Xianyu, G. Hu, and X. Jiang, Biomicrofluidics **7**, 11802 (2013).
[19]N. Nivedita and I. Papautsky, Biomicrofluidics **7**, 054101 (2013).
[20]S. S. Kuntaegowdanahalli, A. S. Bhagat, and I. Papautsky, Lab Chip **9**, 2973 (2009).
[21]K. Aran, A. Fok, L. A. Sasso, N. Kamdar, Y. Guan, Q. Sun, A. Ündar, and J. D. Zahn, Lab Chip **11**, 2858 (2011).
[22]S. Zheng, H. Lin, J.-Q. Liu, M. Balic, R. Datar, R. J. Cote, and Y.-C. Tai, J. Chromatogr. A **1162**, 154 (2007).
[23]V. Vandelinder and A. Groisman, Anal. Chem. **78**, 3765 (2006).
[24]P. Wilding, L. J. Kricka, J. Cheng, G. Hvichia, M. A. Shoffner, and P. Fortina, Anal. Biochem. **257**, 95 (1998).
[25]Y. Nam, M. Kim, and T. Kim, Sens. Actuators, B **190**, 86 (2014).
[26]T. G. Kang, Y.-J. Yoon, H. Ji, P. Y. Lim, and Y. Chen, J. Micromech. Microeng. **24**, 087001 (2014).
[27]J. Alvankarian, A. Bahadorimehr, and B. Yeop Majlis, Biomicrofluidics **7**, 014102 (2013).
[28]T. F. Didar, K. Li, M. Tabrizian, and T. Veres, Lab Chip **13**, 2615 (2013).
[29]T. F. Didar, K. Li, T. Veres, and M. Tabrizian, Biomaterials **34**, 5588 (2013).
[30]M. Hosokawa, T. Yoshikawa, R. Negishi, T. Yoshino, Y. Koh, H. Kenmotsu, T. Naito, T. Takahashi, N. Yamamoto, Y. Kikuhara, H. Kanbara, T. Tanaka, K. Yamaguchi, and T. Matsunaga, Anal. Chem. **85**, 5692 (2013).
[31]M. Hosokawa, M. Asami, S. Nakamura, T. Yoshino, N. Tsujimura, M. Takahashi, S. Nakasono, T. Tanaka, and T. Matsunaga, Biotechnol. Bioeng. **109**, 2017 (2012).
[32]H. Wei, B. H. Chueh, H. Wu, E. W. Hall, C. W. Li, R. Schirhagl, J. M. Lin, and R. N. Zare, Lab Chip **11**, 238 (2011).
[33]R. Schirhagl, I. Fuereder, E. W. Hall, B. C. Medeiros, and R. N. Zare, Lab Chip **11**, 3130 (2011).

[34]X. Li, W. Chen, G. Liu, W. Lu, and J. Fu, Lab Chip **14**, 2565 (2014).
[35]H. M. Ji, V. Samper, Y. Chen, C. K. Heng, T. M. Lim, and L. Yobas, Biomed. Microdevices **10**, 251 (2008).
[36]X. Chen, D. F. Cui, C. C. Liu, and H. Li, Sens. Actuators, B **130**, 216 (2008).
[37]J. S. Shim, A. W. Browne, and C. H. Ahn, Biomed. Microdevices **12**, 949 (2010).
[38]M. A. Unger, H. P. Chou, T. Thorsen, A. Scherer, and S. R. Quake, Science **288**, 113 (2000).
[39]M. Du, X. Ye, K. Wu, and Z. Zhou, Sensors (Basel) **9**, 2611 (2009).
[40]M. Du, Z. Ma, X. Ye, and Z. Zhou, Sci. China Technol. Sci. **56**, 1047 (2013).
[41]M. Gironès, R. G. H. Lammertink, and M. Wessling, J. Memb. Sci. **273**, 68 (2006).
[42]K. Aran, L. A. Sasso, N. Kamdar, and J. D. Zahn, Lab Chip **10**, 548 (2010).